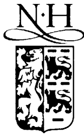
ELSEVIER

Nuclear Instruments and Methods in Physics Research B 181 (2001) 199–210

NIM B
Beam Interactions with Materials & Atoms

www.elsevier.com/locate/nimb

Nuclear emission microscopies

B.L. Doyle [a,*], D.S. Walsh [a], S.N. Renfrow [a,b], G. Vizkelethy [a,1], T. Schenkel [c], A.V. Hamza [d]

[a] *Sandia National Laboratories, Org. 1111 MS-1056, P.O. Box 5000, Albuquerque, NM 87185-1056, USA*
[b] *Mission Research Corporation, Huntsville, AL, USA*
[c] *Lawrence Berkeley National Laboratory, Berkeley, CA, USA*
[d] *Lawrence Livermore National Laboratory, Livermore, CA, USA*

Abstract

Alternatives to traditional nuclear microprobe analysis (NMA) emerged two years ago with the invention of ion electron emission microscopy (IEEM). With nuclear emission microscopy (NEM) the ion beam is only partially focused so as to fill the field of view of a special emission particle microscope system fitted with a single particle position sensitive detector (PSD). When a single ion strikes the sample, the emitted secondaries (e.g. electrons, photons, ions, etc.) are projected at great magnification onto this PSD where position signals are generated. These X and Y signals are then put into coincidence with other signals made by this same ion in a fashion completely analogous to traditional nuclear microprobe analysis. In this paper, an update will be given on the state of NEMs, which currently includes IEEM and highly charged ion–secondary ion mass spectroscopy (HCI–SIMS). In addition, a new type of full-field nuclear imaging is proposed: ion photon emission microscopy or IPEM. © 2001 Elsevier Science B.V. All rights reserved.

PACS: 61.85.JH; 85.30.TV; 61.16.YC; 78.60.Hk
Keywords: Nuclear emission microscopy; Ion photon emission microscopy; Ion electron emission microscopy; Highly charged ion–secondary ion mass spectroscopy

1. Introduction

A radically new form of nuclear microscopy, nuclear emission microscopy (NEM), was invented by Sandia two years ago to address the problem of performing single-ion nuclear microprobe analysis (NMA) using ions that are difficult, or even impossible, to focus with conventional nuclear microprobes [1]. The basic premise of NEM is that it is sometimes easier to determine where an unfocused ion hits a sample rather than focus and scan an ion to a prespecified location. The specific challenge Sandia was facing was the execution of radiation effects microscopy [2,3] to measure single event effects (SEEs) on integrated circuits using high linear energy transfer (LET) beams from the Sandia Tandem-radio frequency quadrupole

* Corresponding author. Tel.: +1-505-844-7568; fax: +1-505-844-7775.
E-mail address: bldoyle@sandia.gov (B.L. Doyle).

[1] On leave from Idaho State University, Pocatello, ID, USA.

0168-583X/01/$ - see front matter © 2001 Elsevier Science B.V. All rights reserved.
PII: S 0 1 6 8 - 5 8 3 X (0 1) 0 0 5 3 5 - 3

(RFQ) accelerator. Fig. 1 compares the surface LET, depth of penetration (both in Si) and mass-energy products of beams from several US accelerators used for SEE testing. The highest LET ions of most accelerators, including the Sandia Tandem-RFQ, used for SEE measurements, have very high magnetic rigidity and poor energy chromaticity which makes microfocusing quite problematic. In addition some of these ions can easily penetrate the tips of the object and aperture slits used to define these beams, which further deteriorates the spatial definition of such beams.

The first NEM was called ion electron emission microscopy or IEEM [1]. With IEEM, the ion beam is not focused, but instead, the secondary electrons made by each ion on the target are project imaged through the lenses of a photoelectron emission microscope (PEEM) onto a single electron position sensitive detector (PSD). The signals from this PSD then records the strike point of the ion on the target, thereby ameliorating the need to focus the incident ion beam. After producing secondary electrons on the surface of the sample, the ion continues to penetrate into the semiconductor or device under test where it deposits charge, and potentially produces an SEE [4].

Coincidentally, a second NEM was developed by LLNL almost simultaneously with IEEM which is called highly charged ion–secondary ion mass spectroscopy (HCI–SIMS) [5]. HCI–SIMS is actually quite similar to IEEM in that secondary electrons are also project imaged to provide the ion strike point, but in this case the incident ions are lower-energy highly charged ions from an electron beam ion trap (EBIT), and the detected signal is the measurement of the time of flight of secondary ions produced during the interaction of these ions with the sample surface. HCI–SIMS is therefore an NEM that images surface composition.

In this paper, an update is given on the status of the two existing types of NEM: IEEM and HCI–SIMS. A new full field nuclear microscopy being developed at Sandia, ion photon emission microscopy (IPEM) is also proposed. IPEM will be virtually identical to IEEM, with the exception that single-ion-induced photons are projection imaged, instead of electrons. Some of the first proof-of-concept experiments for IPEM will be discussed, as will the potential future utility of IPEM. One of the most exciting predictions regarding IPEM is that it could be performed with radioactive sources in air, utilizing a standard optical microscope (OM).

2. Nuclear emission microscopies

Single-ion nuclear microscopy normally involves focusing a low intensity (a few fA) MeV-

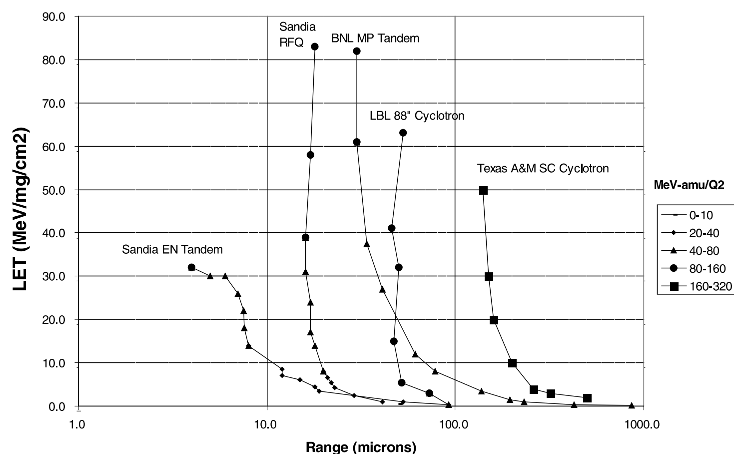

Fig. 1. Linear energy transfer (LET), ion range and mass-energy product for beams from several US accelerator labs used for radiation effects testing of integrated circuits.

energy ion beam to micron or even submicron dimensions, steering this beam to a specific (X, Y) position on the sample specimen, and measuring an analysis signal such as ion beam-induced charge collection (IBICC) produced when an individual ion enters into the sample. We could as well be discussing SEU-imaging, time resolved (TR)I-BICC, ion microbeam tomography, the detection of sputtered ions (SIMS), or any IBA involving single incident ions. These analysis signals are typically recorded as a pulse height (S) at that position. The process is then repeated at a new (X, Y) position, which is reached by scanning the beam in a type of "flying spot" analysis. A schematic of this form of NMA is shown in Fig. 2(a). The data from such an experiment is usually collected in list-mode, i.e. a file of $\{X, Y, S\}$ events, which is later analyzed off line.

As indicated above, an alternative to this traditional style of nuclear microprobe analysis emerged two years ago with the introduction of NEMs, the first being IEEM. With this new type of microscopy (shown in Fig. 2(b)), the ion beam is either unfocused or only partially focused so as to fill the field of view of a special lens system that witnesses the ion–solid interaction that occurs at or near the sample surface. When a single ion strikes the sample, the emitted particles (electrons, photons, ions, etc.) are projected at great magnification onto a highly sensitive PSD which generates X_p and Y_p signals. In some cases, a thin coating optimized to produce large numbers of these particles is applied to the sample surface. These PSD signals are then put into coincidence with the analysis signal (S) made by this same ion, inside the sample, and an $\{X_p, Y_p, S\}$ event file is created. This file is virtually identical to the $\{X, Y, S\}$ list made by traditional nuclear microscopy.

NEM is distinguished from other full field microscopies [6], such as PEEM, low energy electron microscopy (LEEM), or stigmatic imaging secondary ion mass spectrometry (SIMS), because it relies on the combination of two completely unrelated signals: the emission particles from the coating layer which is used only to determine (X, Y) and the measurement event signal created inside the sample (e.g. IBICC). With other full field microscopies, the emitted particles carry not only the (X, Y) position information, but also the information being measured by the analysis (e.g. work function variations with PEEM, surface steps with LEEM, and composition with SIMS). HCI–SIMS fits somewhere in the middle of these two types of emission microscopies because the emitted particles (electrons and ions) used for

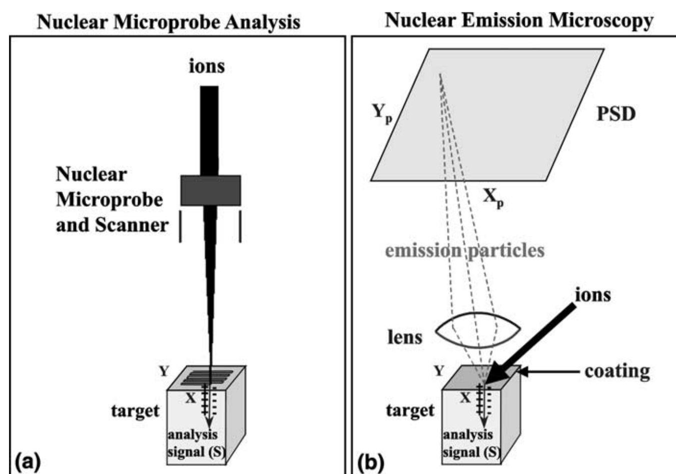

Fig. 2. Schematic comparison of traditional "Flying Spot" nuclear microprobe analysis where the ion beam is focused and scanned, and ion-induced emission microscopy where the beam is not focused, but instead emission particles produced by each ion are project imaged.

position also provide the start pulses used in the time-of-flight analysis.

One of the great attributes of the traditional NMA is that each and every ion can produce an analysis signal (e.g. IBICC). This unity detected event probability guarantees that this type of analysis minimizes the amount of radiation damage to the sample. This is not necessarily the case with the NEM method, as has been discussed previously [1]. To illustrate this, refer to Fig. 2(b). When the individual ion strikes the sample lets say that γ emitted particles are produced. The successful detection of these particles by the PSD depends on the collection and transmission efficiency, ϵ, of the projection microscope lens system together with the detection efficiency, δ, of the PSD. So, of the γ particles produced by the ion on the sample, only $\gamma\epsilon\delta$ are detected. Several limiting cases, numbered (1–4), then present themselves.

1. If $\gamma\epsilon\delta \ll 1$, count rates could become so low that the associated long analysis times or huge damage levels would preclude this application.
2. If $\gamma\epsilon\delta < 1$, then NEM will have a lower count rate than NMA for the same beam current. This means that for the same data quality (i.e. statistics), the sample will suffer from more radiation damage with NEM. This may or may not represent a problem.
3. If $\gamma\epsilon\delta > 1$, then the quality of data from the NEM and NMA analysis and the degree of radiation damage should be comparable. For this case multiple particles will be detected for each ion, but they all originate from the same point and therefore do not confuse the PSD.
4. If $\gamma\epsilon\delta \gg 1$, then so many emission particles can potentially be detected, that closing the apertures in the microscope (to improve resolution) will have no cost in count rate, that is until $\gamma\epsilon\delta = 1$. It is in this situation that NEM has the potential of providing superior resolution as compared with NMA.

3. Examples

There are currently three NEMs at various stages of development: IEEM, IPEM and HCI–SIMS Table 1 summarizes attributes of each of these NEMs.

3.1. Ion electron emission microscopy

Referring to Fig. 2(b) and [1], with IEEM a beam of MeV ions, provided by an accelerator, impinges on a semiconductor sample (currently at an angle of 75° with the surface normal) which is usually coated with a thin metal layer to enhance production of secondary electrons. The secondary electrons which are generated by each ion (and shown to originate at X, Y in Fig. 2(b)) are then accelerated and projected using the lens system of a PEEM. The incident "flood" ion beam is usually partially focused with a magnetic quadrupole lens, so as to fill the field of view of the PEEM. These electrons are refocused to positions X_p and Y_p at the projection focal plane of the PEEM and recorded with a microchannel plate + resistive anode encoder PSD. Two electronic pulses with voltages proportional to X_p, Y_p are generated by the PSD,

Table 1
Properties of nuclear emission microscopies

NEM	Beam	Energy (MeV)	Emitted particle	γ	ϵ	δ	Detected particle/ion	Detected signal	Property measured	Resolution (μm)
IEEM	He	6	e–	4	0.1	0.5	0.2	IBICC,...	Elec. properties	1
	Au	380	e–	360	0.1	0.5	18	IBICC,...	Elec. properties	0.1
IPEM	He	6	Photon	2000	0.0002	0.25	0.1	IBICC,...	Elec. properties	1
HCI–SIMS	Xe^{48+}	0.7	e–	100	0.1	0.5	5	Sputtered – ion	Surface compo	0.8
HCI–SIMS	Xe^{48+}	0.7	H+	10	0.1	0.5	0.5	Sputtered + ion	Surface compo	2

and these signals are then put into coincidence with the analysis signals (shown schematically as IBICC in Fig. 2(b)) using a multiparameter data acquisition system. Each event is stored as an $\{X_p, Y_p, S\}$ record in list mode.

Hasselkamp et al. [7] have shown that the number of secondary electrons (γ_e) produced by each ion can be expressed as

$$\gamma_e = \Lambda(\mathrm{d}E/\mathrm{d}x) \qquad (1)$$

for ions on metals at normal incidence. Λ ranges from 0.07 to 0.13 for various ions on smooth silver targets when the stopping power is expressed in units of eV/Å. The values of γ listed in Table 1 for IEEM using beams of 6 MeV He and 380 MeV Au were obtained using scaled stopping powers [8] for these ions on Ag and assuming $\Lambda = 0.1$. In [1] we measured the total system detection efficiency to be 0.05 using protons on Au-coated PIN diodes and selecting the largest aperture in the PEEM (300 μm). This indicates that for a PSD efficiency of $\delta = 0.5$, that $\epsilon = 0.1$, and these values are also listed in the table. The detected particles per ion, which in this case are electrons, will range from ~0.2 to almost 20 for IEEM using ions at normal incidence. For a 75° tilt, γ_e increases by a factor of ~4 according to the Hasselkamp theory. The resolution of IEEM was measured to be 0.9 μm using the 300 μm aperture in the PEEM lens.

This analysis suggests that for the largest PEEM aperture, that using He ions at normal incidence will fall under case (2) above where micron-level resolution can be obtained, but with ~5× more beam-induced damage to the sample. Using He ions incident at 75° will fall into case (3) where IEEM and NMA are essentially equivalent. The use of Au ions falls into case (4), where multiple electrons are detectable, and this indicates that smaller PEEM apertures could be used to improve the 0.9 μm resolution. If a 70 μm aperture is used, the detected electrons/ion should drop to 1 and the resolution should improve to ~ 0.2 μm.

A good example of IEEM data is shown in Fig. 3. A ~1 fA, 5 MeV He beam at 75° incidence was used to produce these images for a prototype

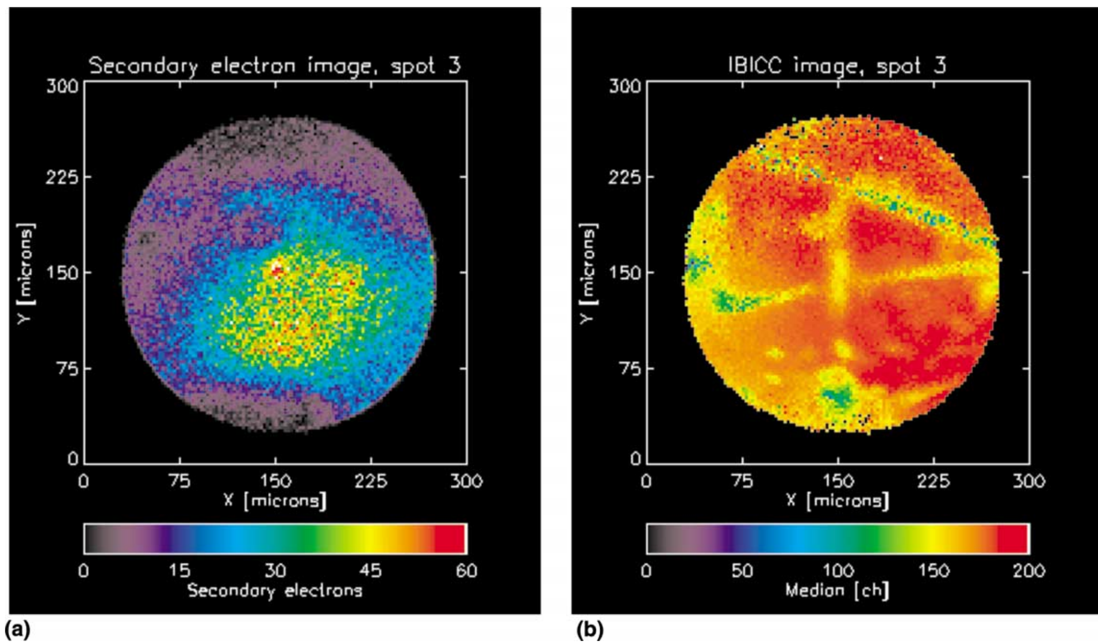

Fig. 3. Ion electron emission microscopy (IEEM) images of (a) 20 MeV C secondary electron intensity and (b) ion beam-induced charge collection (IBICC) medians for a CdZnTe detector. While the beam was partially focused into the parallelogram shown in (a), the IBICC image in (b) is completely filled.

Au-coated cadmium zinc telluride (CZT) γ-ray detector. Fig. 3(a) shows the secondary electron intensity map. The partial focus of the beam can easily be discerned as the bright parallelogram near the center region of this image. Note that there are counts at the 1–2 electrons per pixel level outside this region due to the incomplete focus of the beam or halo effects. In Fig. 3(b) we plot the IBICC map collected using the (X, Y) position information of the secondary electrons in Fig. 3(a) in conjunction with the IBICC pulses measured from this sample. The median of the IBICC pulse height distribution at each (X, Y) position pixel is being plotted in this figure. It is interesting to note that while the quality of the IBICC image is best in the region of the partial focus, structure can even be observed outside this area where the beam intensity was extremely low. While this particular sample did not demonstrate significant beam damage effects, the fact that an image can be seen in the halo region surrounding the beam spot indicates that considerably less beam exposure could have been used to obtain this data. While it is not currently clear whether the variations in this IBICC signal are due to defects in the Au layer or the CZT crystal, it is apparent from this figure that IEEM–IBICC can provide data of nearly the same quality as a scanned nuclear microprobe.

Unfortunately, this was not found to be the case when examining ICs with IEEM–IBICC images taken with 5 MeV He on a Sandia TA-780 16K SRAMs. While individual transistors were clearly defined using traditional microbeam IBICC, they could not be resolved with the IEEM–IBICC. This was probably due to the fact that the He ion beam used in this experiment impinged at an angle of 75° to the surface normal. Since the emitted electrons come off at normal incidence, this IBICC image suffers from a type of parallax where the projected trajectory of the ion within the sample, and which causes the IBICC event, does not correspond to the generation point of the corresponding electrons.

3.2. Ion photon emission microscopy

A natural extension of IEEM is to use ion-induced photons (ionolumenescence) to record the arrival point of ions onto a sample. This technique is called IPEM. Anyone who has used a quartz to view an ion beam of an accelerator has performed a crude form of IPEM where, referring to Fig. 2(b), the coating on the sample is the quartz, the emitted particles are photons, the lens is in your eye, the PSD is your retina, and the analyzer is your brain! To our knowledge, no one has actually performed an IPEM experiment where an ion induced signal in the target is correlated with the position where photons are created. This is therefore the first time such a system has been proposed. We present here, proof of principle experiments where γ, ϵ and δ are determined for IPEM, and then predict the performance characteristics of a system which is currently under development at Sandia.

Refer to Fig. 2(b) for the following discussion. With IPEM the beam of MeV ions (from an accelerator or radioactive source) impinges on a sample which is coated with a thin phosphor layer to enhance production of photons. The photons generated by each ion are then collected and projected using the lens system of an optical microscope (OM). We are currently using the JEOL OM-40 in-vacuo OM that is also used for front-viewing applications on our conventional nuclear microprobe. This particular microscope has a 1 mm hole in a prism followed by the objective lens through which the beam passes to the target at normal incidence. The photons generated by the beam are (1) collected and made parallel by this same lens, (2) passed to the prism where they are bent 90° and away from the beamline, (3) passed to another prism and another 90° bend, and (4) on to the eyepiece lens which focuses the photons onto the single photon PSD. In the future, this single photon PSD will consist of a bialkali photon–electron converter + microchannel plate + resistive anode encoder, but currently we are just using a Hamamatsu miniaturized photo multiplier tube (PMT). This PMT can detect single photons, but cannot resolve their position. The rest of the data acquisition follows that of the IEEM [1] which correlates an analysis signal(s) with the X, Y signals from the PSD.

A companion paper [9] gives details of our quest to find the optimum phosphor coating for

IPEM. In general, we have observed that for standard phosphors the number of photons detected per incident ion ranges from ~0.2 to ~10 for thick phosphors, and ~0.04 for thin phosphor blades.

The Birks ionoluminescence [10] theory gives

$$\gamma_p = (dL/dx)X, \quad (2)$$

where

$$\frac{dL}{dx} = \frac{P(dE/dx)}{1 + \beta(dE/dx)} \quad (3)$$

and P is the number of photons produced per MeV (16 666 for anthracene), dE/dx is in units of MeV/μm, β represents a saturation in luminescence and is in units of microns/MeV (117 for anthracene), and X is the thickness of the phosphor in microns. Using scaled stopping powers [8] and an anthracene phosphor layer 20 μm thick (anthracene is an organic crystal to which other phosphors are often compared), the number of photons made by each 6 MeV He ion, γ_p is 2000. Because Eq. (3) is already in saturation for He, Au ions only produce a modest increase in photon generation. The collection–transmission efficiency of the OM-40 is $\epsilon \sim 0.0002$, and the efficiency of the PSD will be in the $\delta \sim 0.2$ range. The number of photons/ion will then be ~0.1 for an average 20 μm phosphor, for either He or Au ions. This places IPEM in case (2) above, for both the He and Au ions, where increased ion damage is an issue. We expect IPEM to move to case (3) or even (4) when optimum phosphor coating layers or improved photon projection systems are developed.

An experimental test of IPEM was made using the Sandia nuclear microprobe and the OM-40 microscope fitted with a PMT. A 20 MeV C beam was focussed and then scanned across a sample consisting of a PIN diode coated with 5–10 μm of a very nonuniform $SrGa_2S_4$:Eu thiogallate phosphor (used for green in commercial projection TVs) deposited by sedimentation. The position of the ions striking the sample was controlled by the Sandia microbeam focussing and steering system, and not by detecting the position of the photons using a PSD. In fact, IPEM would never work very well with such a ceramic polycrystalline phosphor because the lateral resolution would be determined by the crystallite size and other light scattering effects, rather than the microscope + PSD resolution. Nevertheless, ion beam-induced luminescence (IBIL) and IBICC images were made by combining the pulse height signals generated by both the PMT and PIN diode with the X, Y scan position, and these images are plotted in Figs. 4(a) and (b). Fig. 4(a) plots the median of the PMT output versus X, Y which approximately corresponds to the number of photons per ion versus X, Y. The phosphorescence of thiogallate has a lifetime of only ~0.2 μs when excited with C ions, and therefore most of the photons generated, by each ion, are collected as a single pulse in the PMT and associated electronics, in a fashion similar to pile-up. The blue region represents single photon detection presumably from thin regions while the yellow areas indicate as many as 3–4 photons are being collected, all at once, from thicker regions. Thallogallate is known to be much brighter than anthracene, as demonstrated by these data. Fig. 4(b) shows a medium filtered IBICC image made simultaneously with Fig. 4(a). Here the contrast is reversed: the yellow regions have the highest IBICC medians, and therefore are regions of the thinnest phosphors; whereas, the blue areas have the lowest energy IBICC signals, and demonstrate the greatest energy loss from passage through thick phosphor regions. The black areas in both images show a lack of coincidences, which means that no phosphor was present in these areas. While this experiment is not exactly IPEM, it does demonstrate the viability of this new emission microscopy.

It is clear that superior phosphors will be required to fully realize the potential of IPEM. These phosphors should have the following attributes:

1. be thin (<5 um) (so that ions can easily penetrate into the sample);
2. be easy to apply (to facilitate sample preparation);
3. have high brightness (i.e. photons/ion/μm);
4. be clear and continuous (to avoid photon-blooming due to scattering from defects);
5. have a low index of refraction (to increase the collection angle);

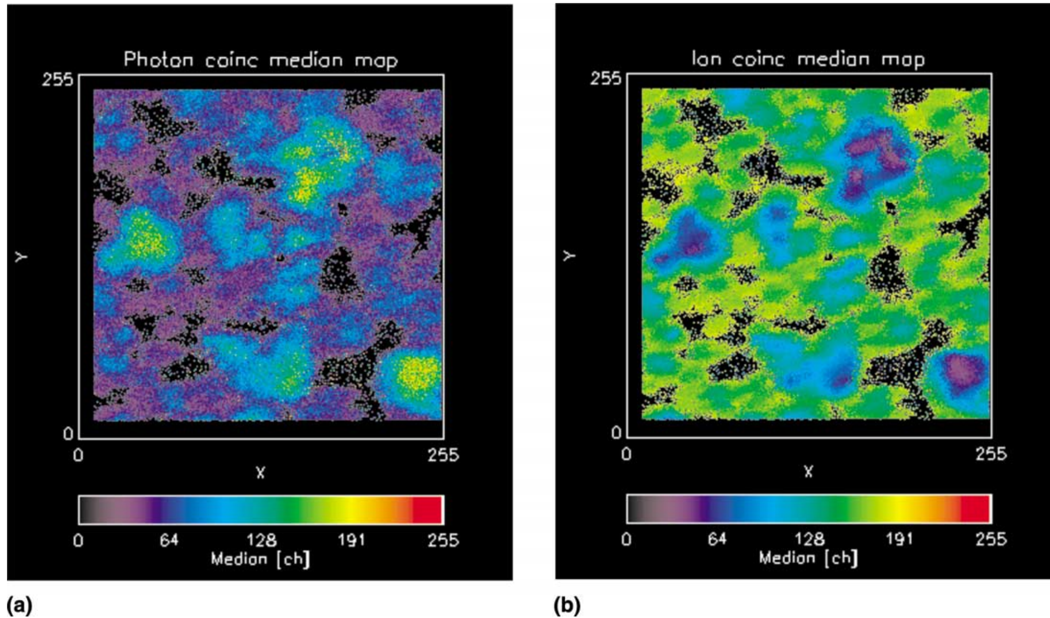

Fig. 4. Ionolumenscence and IBICC median images of a thiogallate phosphor using 20 MeV C ions: (a) plots the median of the PMT output which corresponds to the number of photons per ion (e.g. blue represents single photon detection from thin regions while the yellow areas indicate as many as 3–4 photons are being collected from thicker regions); (b) shows a medium filtered IBICC image, and here the contrast is reversed: the yellow areas with high IBICC medians are for regions of the thinnest phosphors, and visa versa for the blue low median IBICC regions.

6. emit at an optimum wavelength (so the PSD has high efficiency);
7. possess an attenuation coefficient comparable to the film thickness (to reduce multiple scattering induced broadening).

Much work is being undertaken to find the optimum phosphor for IPEM [9]. Once this phosphor is determined, the OM-40 at Sandia will be fitted with a single photon PSD and true IPEM will be performed.

3.3. Highly charged ion–secondary ion mass spectoscopy

Highly charged ions (HCI), like Xe^{48+} or Au^{69+}, with velocities below the Bohr velocity, or kinetic energies $\leqslant 5$ keV/u, have charge states far in excess of the mean equilibrium charge state that corresponds to the velocity with which they impinge on a solid target. The latter is about 1+. Measurements with thin foil targets have shown that charge state equilibrium is established within a few fs [11,12]. During this time, the potential energy associated with the initial charge state is deposited close to the target surface. In the example of Au^{69+} with a kinetic energy of a few hundred keV, a potential energy of 170 keV is deposited along a path of about 50 Å in amorphous carbon. The mean energy deposition rate of about 3.4 keV/Å is close to the SRIM value of the maximum electronic stopping power for 600 MeV gold ions in carbon (2.6 keV/A). The intense, localized and ultrafast electronic excitation of a surface by the equilibration of a slow, HCI results in high yields of secondary electrons, positive and negative secondary ions as well as molecular ions. These high yields are used to image surfaces in the HCI based emission microscope that was developed at Lawrence Livermore National Laboratory [5,11].

Again referring to Fig. 2(b), with HCI–SIMS the incident HCIs are produced in an EBIT, and accelerated as a flood beam to the sample. An objective (immersion) lens accelerates the particles emitted at the surface, which in this case are either

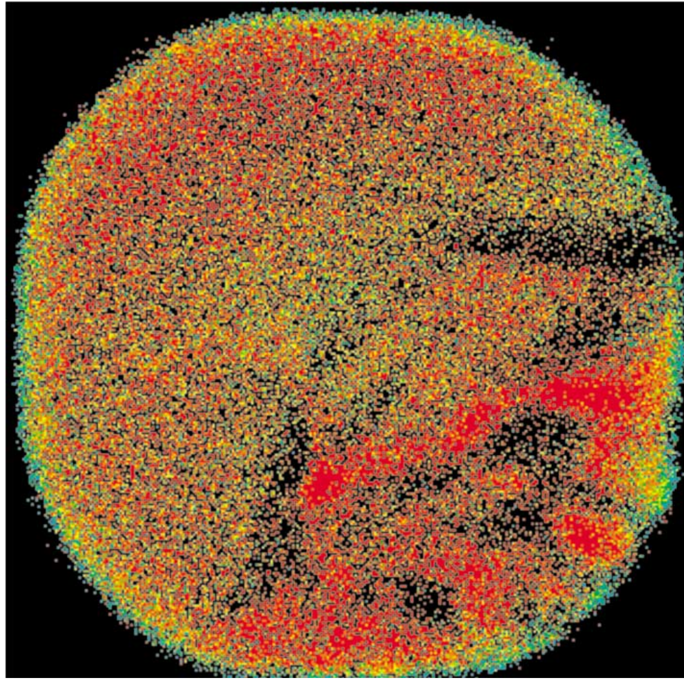

Fig. 5. Image of a scratch on a quartz lens based on electron emission yield contrast. The field of view is 0.45 mm, the magnification was 90×. Charging of the target was suppressed with a pulsed, low energy electron gun.

secondary electrons (like IEEM) or H+ ions (H is ubiquitous on sample surfaces) through the flight tube to a position sensitive micro channelplate detector (PSD). The flight time between start pulses from electrons (in negative polarity) or protons (in positive polarity) and stop pulses from trailing secondary ions is used to determine the mass-to-charge ratio of the secondary ions. Secondary electron yields of a few hundred have been observed using HCI–SIMS [11]. Here, the process is potential electron emission, but the secondary electron yields are actually consistent with the above-mentioned Hasselkamp theory of kinetic electron emission (Eq. (1)) and an effective stopping power of 3.4 keV/Å. For positive-mode HCI–SIMS, the γ for protons is $\sim$10. These values and lens and PSD performance are listed in Table 1. It can be seen in this table that HCI–SIMS for negative ion analysis falls into case (4), whereas case (3) applies for positive ions. Using slow, HCIs as projectiles also has the potential to increase sensitivity due to increased ionization probabilities of secondary ions [13].

The first prototype instrument has demonstrated a resolution of 800 nm in the imaging of copper lines on silicon based on secondary electron contrast [5]. In positive polarity, a resolution of 2 μm was achieved. The investigation of resolution limiting factors is in progress.

The fact that multiple secondary ions are emitted for individual projectiles allows the application of coincidence counting to HCI–SIMS [14–16]. Here, time-of-flight cycles are started by the impact of an individual HCI and streams of secondary ions associated with this start pulse are stored in a list. After accumulation of a few million cycles, the list can be searched for TOF-cycles in which a specific secondary ion was detected. Summation of all these cycles now shows other secondary ions that were emitted from individual projectiles together with the specified secondary ion. Through this analysis of secondary ion coincidences, information is gathered on the nano-environment of a selected species. The length scale of the composition information is given by the area

from which one HCI emits secondary ions. We estimate the latter to be 10–20 nm in diameter. This effective resolution is similar to the practical limit in focused ion beam SIMS [17]. HCI–SIMS with coincidence analysis has been applied to the characterization of processing steps in semiconductor manufacturing.

In Fig. 5, we show an example of a relatively low resolution image of a scratch on a quartz lens with 700 keV Xe^{48+} ions. Contrast is based on secondary electron emission. Charge compensation was achieved with a pulsed low energy electron gun. Spectra of negative secondary ions collected in parallel with the electron pulse height image are shown in Fig. 6. The top spectrum shows secondary ions emitted from the scratched region. The spectrum from the unscratched region (bottom) exhibits large peaks of surface contaminants. An important and challenging problem that is being addressed with HCI emission microscopy is that of damage mechanisms in optical components exposed to high power lasers. Here, the integration of coincidence analysis with emission microscopy at improved resolution holds the promise to enable significant advances.

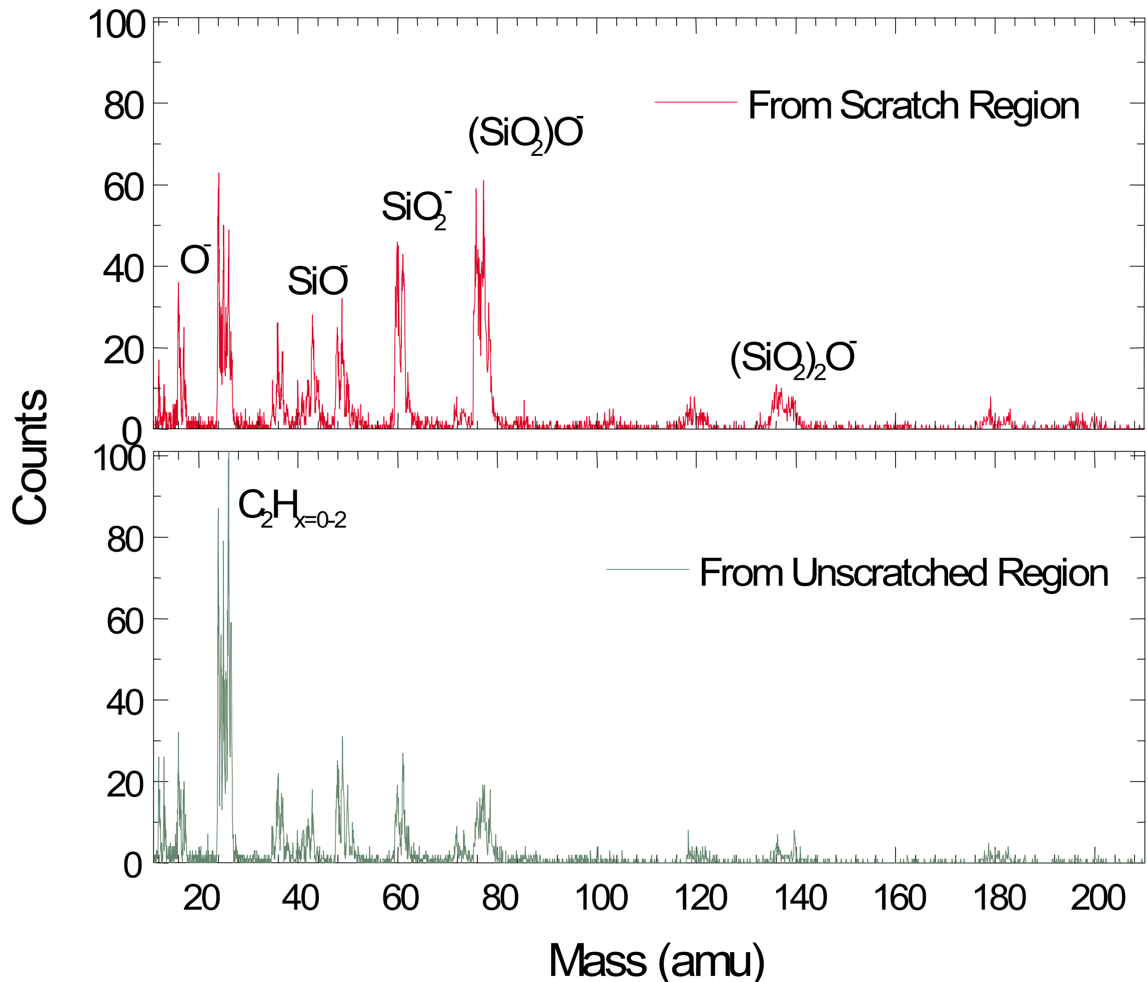

Fig. 6. Negative secondary ion spectra collected from scratched (top) and unscratched (bottom) regions in the image.

4. Conclusion and future directions

It is clear from the above that NEM will play an increasingly important part in the future evolution of nuclear microscopy. IEEM is already starting to be used for radiation effects microscopy of ICs and semiconductors. IPEM should provide an extremely simple platform to microscopically study the electronic properties of semiconductors. HCI–SIMS is proving to be a highly sensitive new surface analysis where, by using the mass-coincidence technique, particulates of only a few nm in size can be studied.

While the underlying motivation to develop these NEMs was to avoid focusing the beam, an additional advantage is now becoming apparent: Radioactive alpha or fission sources could potentially be combined with NEM to even eliminate the need for an accelerator. For example, an alpha-source IEEM would be quite compact, and trivial to implement in a laboratory associated with an IC manufacturing line, semiconductor R&D facility, or any laboratory which does not possess an accelerator, but is interested in performing single-ion nuclear microscopy. One of the most exciting predictions regarding IPEM is that it could be performed in air with an alpha particle source coated onto the objective lens of an OM, and replacing the CCD with a single photon PSD.

It is important to point out here that NEMs are not being proposed as a replacement to traditional nuclear microprobes, but that they do offer an attractive alternative in certain very specialized applications. Because of the low count rate capability of virtually all PSDs (<1 Mcps), these applications must be made with beam currents <100 fA. Very few routine IBA techniques can be performed with such low beam currents. Until the bandwidth of PSDs increases dramatically, NEMs will therefore be limited to techniques which generally fall under the heading of single-ion nuclear microscopy, such as the various radiation effects microscopies, ion transmission microscopies and SIMS, all which have a near unity detected event probability.

Future developments of these NEMs which are expected to occur in the next few years include:

IEEM – The only way to resolve the parallax problem is to use ions that impinge on the sample at normal incidence, and we are in the process of rebuilding the IEEM to do exactly that. This second generation IEEM will transmit the MeV ion beam directly through an annular PSD, through the PEEM lens system and onto the sample. Specially designed ion collimators have been positioned within the PSD to prevent beam ions from triggering the PSD. The low electric fields used to focus the secondary electrons are expected not to affect the trajectory of the MeV ions. The system is also being reassembled on the RFQ booster system.

IPEM – A Quantar single photon PSD is being acquired which has 70 μm resolution. This PSD will replace the PMT on the OM-40 and should provide a final resolution in the 0.5 μm range. This first IPEM system will then be tested on samples which have been coated with the optimum phosphor layer determined by the Sandia–UNT–INFN collaboration [9]. After this test, we plan to coat an alpha particle source onto the objective lens of a high power OM, and replace the CCD with the Quantar single photon PSD. Such a system should be able to perform IPEM for radiation microscopy applications in air, with an instrument of low cost (<$60 K) and tabletop footprint.

HCI–SIMS – Two groups at LLNL and LBNL are pursuing the continued development of this NEM. Initial applications are expected to be found in the IC industry, for example, to measure the composition of nm-sized particulates which can reduce production yields. These groups are also exploring a compact alternative to the huge accelerator systems typically used for the generation of high LET beams with energies around 1 MeV/u which involves the integration of an EBIT as a source for HCIs (Fe^{26+}, Xe^{52+} to Au^{77+}) into the terminal of a 2–3 MV $\times q$ accelerator structure.

Acknowledgements

Work at Sandia supported by the US DoE under contract DE-AC04-94AL85000. Work at LBNL was supported by the Director, Office of Basic Energy Sciences, of the US Department of Energy under Contract No. DE-AC03-76SF00098.

Work at LLNL was performed under the auspices of the US Department of Energy under contract No. W-7405-ENG-48.

References

[1] B.L. Doyle, G. Vizkelethy, D.S. Walsh, B. Senftinger, M. Mellon, Nucl. Instr. and Meth. B 158 (1999) 6.
[2] K.M. Horn, B.L. Doyle, D.S. Walsh, F.W. Sexton, Scanning Microsc. 5 (1991) 969.
[3] M.B.H. Breese, Mater. Sci. Eng. B–Solid State Mater. Adv. Technol. 42 (1996) 67.
[4] G.C. Messenger, M.S. Ash, Single Event Phenomena, Chapman & Hall, London, 1997.
[5] A.V. Hamza, A.V. Barnes, E. Magee, M. Newman, T. Schenkel, J.W. McDonald, D.H. Schneider, Rev. Sci. Instrum. 71 (2000) 2077.
[6] O.H. Griffith, W. Engel, Ultramicroscopy 36 (1991) 1.
[7] D. Hasselkamp, K.G. Lang, A. Scharmann, N. Stiller, Nucl. Instr. and Meth. 180 (1981) 349.
[8] J. Zigeler, Appl. Phys. Lett. 31 (1977) 544.
[9] C. Yang, B.L. Doyle, P. Rossi, M. Wigam, M. El Bouanani, J.L. Duggan, F.D. McDaniel, Nucl. Instr. and Meth. B 181 (2001) 329.
[10] J.B. Birks, The Theory and Practice of Scintillation Counting, Pergamon, Oxford, 1964.
[11] T. Schenkel, A.V. Hamza, A.V. Barnes, D.H. Schneider, Prog. Surf. Sci. 61 (1999) 23.
[12] M. Hattass, T. Schenkel, A.V. Hamza, A.V. Barnes, M.W. Newman, J.W. McDonald, T.R. Niedermayr, G.A. Machicoane, D.H. Schneider, Phys. Rev. Lett. 82 (1999) 4795.
[13] T. Schenkel, A.V. Barnes, A.V. Hamza, J.C. Banks, B.L. Doyle, D.H. Schneider, Phys. Rev. Lett. 80 (1998) 4325.
[14] A.V. Hamza, T. Schenkel, A.V. Barnes, D.H. Schneider, J. Vac. Sci. Technol. A 17 (1999) 303.
[15] T. Schenkel, M.W. Newman, T.R. Niedermayr, G.A. Machicoane, J.W. McDonald, A.V. Barnes, A.V. Hamza, J.C. Banks, B.L. Doyle, K.J. Wu, Nucl. Instr. and Meth. B 65 (2000) 161.
[16] T. Schenkel, K.J. Wu, H. Li, M.W. Newman, A.V. Barnes, A.V. Hamza, J. Vac. Sci. Technol. B 17 (1999) 2331.
[17] F.A. Stevie, et al., J. Vac. Sci. Technol. B 17 (1999) 2476.